Progress In Electromagnetics Research, Vol. 137, 159–186, 2013

ANALYSIS OF PROPAGATION AND POLARIZATION CHARACTERISTICS OF ELECTROMAGNETIC WAVES THROUGH NONUNIFORM MAGNETIZED PLASMA SLAB USING PROPAGATOR MATRIX METHOD

Xiong Yin[1, 2, *], Hou Zhang[1, 2], Shuji Sun[2], Zhenwei Zhao[2], and Yanli Hu[2]

[1]School of Air and Missile Defense, Air Force Engineering University, Xi'an, Shaanxi 710051, P. R. China

[2]National Key Laboratory of Science and Technology on Electromagnetic Environment, China Research Institute of Radiowave Propagation, Qingdao, Shandong 266107, P. R. China

Abstract—An analytical technique referred to as the propagator matrix method (PMM) is presented to study the problem of electromagnetic (EM) waves interacting with the nonuniform magnetized plasma. In this method, the state vector is proposed to describe the characteristics of eigen waves in anisotropic medium, and state vectors at two different locations are related with each other by the propagator matrix. This method can be used to deal with the phenomenon of the transformation of EM wave polarization induced by anisotropic magnetized plasma, besides the conventional propagation characteristics through plasma slab, which overcomes the drawback of other analytical methods introduced in former studies. The EM problem model considered in this work is a steady-state, two-dimensional, nonuniform magnetized plasma slab with arbitrary magnetic declination angle, which is composed of a number of subslabs. Each subslab has a fixed electron density, and the overall density profile across the whole slab follows any practical distribution function. Based on PMM, a significant feature of strong transformation of EM wave polarization is addressed when an incident wave normally projects on the slab, which leads to the reflected or transmitted waves containing two kinds of waves, i.e., the co-polarized wave and the cross-polarized wave. The effects of varying the plasma parameters on the reflected and transmitted powers of co-polarization and cross-polarization, as well as the absorptive power

Received 4 January 2013, Accepted 6 February 2013, Scheduled 18 February 2013

* Corresponding author: Xiong Yin (yinxiong325@163.com).

for the typical bi-exponential density profile are investigated in detail, which provides a certain reference to various plasma technologies such as plasma stealth and communications through re-entry plasma sheath.

1. INTRODUCTION

Plasma technology is a kind of technology with novel concept and newly working principle, and its latent application in electromagnetic (EM) field is splendid, such as plasma stealth technology [1–3], plasma antennas [4–6], plasma diagnostic [7, 8], plasma photonic crystals [9] and communications through plasma sheath [10–14]. It is very important to find out the mechanism and phenomena about the interactions between EM wave and plasma in the study of this technology. In the past twenty years, a number of analytical and numerical methods have been proposed to investigate the wave propagation in plasma [2, 3, 12–14, 15–21]. Hu et al. [15] used a scattering matrix method to calculate the reflection, transmission and absorption characteristic of EM wave propagation in nonuniform magnetized plasma, where the external magnetized field direction is perpendicular to the direction of EM wave propagation. Pertrin [16] studied the transmission of microwave through magnetoactive plasma layer via the Volume Integral Equation. Soliman et al. [17] have presented the attenuation property about EM wave incidence in nonuniform plasma layers using a multi-mediums method. Huang et al. [18] made a detailed investigation of surface modes at the interface between an isotropic medium and a uniaxial plasma. Lai-Xuan Mao et al. [2, 3] did research on the reflection characteristic of EM wave incidence in non-magnetized closed plasma with outer envelope based on the wave impedance matching principle. Their model considered the double-pass attenuation of the rays inside the plasma slab. Robert M. Manning [12] handled the EM wave propagation process through a flowing plasma immersed in an external magnetic field using the Vlasov equations. In [19], the total internal reflection of a pulsed light beam from vacuum incident upon an ideal non-absorbing plasma was investigated theoretically using the Fourier transform method. Liu et al. [13] and Lei Shi et al. [14] carried out the studies on the transmission solution of EM waves propagation through plasma sheath by adopting the finite difference time-domain (FDTD) method. Yin et al. [20, 21] have utilized the shift-operator finite difference time-domain (SO-FDTD) method to study the reflection and transmission characteristics for a plane wave incident on a magnetized plasma slab. The FDTD method is a more powerful numerical tool for dealing with complicated plasma model compared to analytical methods mentioned

above, but it is a highly time consuming numerical technique due to the usage of massive storage resources required by the problem.

From references above, it can be seen that only propagation characteristics are considered in the problem of EM waves interaction with plasma, while the polarization features are not taken into account. Because these methods mentioned above, except the FDTD method, seem difficulty to deal with the problem of the transformation of EM wave polarization. In fact, some phenomena such as Faraday-rotation or dual-refraction will occur when EM wave propagates in magnetized plasma [22–24], which means magnetized plasma can evidently change the EM wave polarization. Polarization characteristics of scattered EM signals provide important information about physical conditions in the area of localization of the sources and about the medium parameters on the path of wave propagation, so the analysis of the variance of polarization characteristics of EM waves that pass through a magnetized plasma slab is very important in many practical applications such as communication through the plasma sheath and plasma stealth [22–25]. The transformation of EM wave polarization under reflection from thin solid-plasma film on the conditions of plasma resonance was investigated by Bakunov and Zhukov [25]. The variance of the Faraday angle was studied in [23] and [24] by the wave equation incorporated with the nonlinear dielectric function and by the perturbation method, respectively. However, the effect of varying the plasma parameters on the propagation characteristics and the transformation of EM wave polarization had not been discussed simultaneously in these researches.

In this paper, an analytical technique named propagator matrix method (PMM) is presented to study the propagation and polarization characteristics of EM waves interacting with plasma slab. The PMM was firstly used to study heat transfer in spherically stratified media by Negi and Singh [26] and had been extended to the analysis for elastic wave propagation in layered anisotropic media [27] by Rokhlin and Wang. The slab considered in this work is steady-state, nonuniform, collisional and magnetized with arbitrary magnetic declination angle. The electron density distribution model of the plasma slab is represented by a typical bi-exponential profile. Based on PMM, a significant feature of strong transformation of EM wave polarization is addressed when an incident wave normally projects on the nonuniform magnetized plasma slab, which results in the reflected or transmitted waves containing two kinds of waves, i.e., the co-polarized wave and the cross-polarized wave. The deductions of the propagator matrix method are proposed in Section 2. Since this method involves only the manipulation of 4×4 matrices, the

required results can be got very easily. It is demonstrated that this method not only improves accuracy but also produces great speed advantage in comparison with the FDTD method proposed in the recent reference. Numerical results showing the effects of varying the plasma parameters on the reflective and transmitted powers for co-polarization and cross-polarization, as well as the absorptive power are presented in Section 3. Section 4 outlines the important conclusions obtained from the numerical results.

2. PROPAGATOR MATRIX METHOD (PMM) FOR MAGNETIZED PLASMA

2.1. The EM Problem Model and Permittivity Characteristics of the Magnetized Plasma with Arbitrary Magnetic Declination

The geometry of the problem we studied is outlined in Figure 1, where the nonuniform cold magnetized plasma slab indicated as Region **B** is divided into n layers. The thickness of m-th layer and the last one are $z_{m+1} - z_m$ and $z_p - z_n$, respectively. The electron density varies only along z axial direction and the electron density is constant in the same layer but is not equal for different layers. Moreover, the collision frequency is assumed to be identical for all layers of the slab. The external static magnetic field $\mathbf{B}_0$ is in the x-z plane and declines an angle θ_B from z axis. The incident region (0) and transmissive region (p) are free space and denoted as Region **A** and Region **C**, respectively. The plane wave with electric vector polarized in the y direction is incident normally on the slab. The dielectric permittivity tensor $\bar{\varepsilon}$ in the m-th layer of the plasma slab is denoted as $\bar{\varepsilon}_m$ and will be derived by the following procedure.

Assuming that EM fields have time dependent of $e^{j\omega t}$, the constitutive relations between polarized current density vector $\mathbf{J}$ and electric field vector $\mathbf{E}$ for magnetized plasma with arbitrary magnetic declination are given by Refs. [20, 21]

$$\frac{d\mathbf{J}}{dt} + \nu_{en}\mathbf{J} = \varepsilon_0\omega_{p,m}^2\mathbf{E} + \boldsymbol{\omega}_b \times \mathbf{J} \tag{1}$$

$$\mathbf{J} = j\omega\varepsilon_0\bar{\chi}_m \cdot \mathbf{E} \tag{2}$$

$$\bar{\varepsilon}_m = \varepsilon_0\left(\bar{\mathbf{I}} + \bar{\chi}_m\right) \tag{3}$$

where $\bar{\mathbf{I}}$ is a unit tensor, ε_0 the permittivity in vacuum, $\boldsymbol{\omega}_b$ the cyclotron angular frequency, ν_{en} the collision frequency (for both electron-ion and electron-neutral collisions), and $\omega_{p,m}$ and $\bar{\chi}_m$ are the plasma angular frequency (primarily representing electron oscillation

frequency here) and the electric susceptibility tensor for the m-th layer of the magnetized plasma slab shown in Figure 1, respectively. Since $\boldsymbol{\omega}_b$ is proportional to the static magnetic field $\mathbf{B}_0$ [21], it can be decomposed to components along axial directions, viz.,

$$\boldsymbol{\omega}_b = \omega_b \hat{\mathbf{b}} = \omega_b \sin\theta_B \hat{\mathbf{x}} + \omega_b \cos\theta_B \hat{\mathbf{z}} \tag{4}$$

where $\hat{\mathbf{b}}$ is a unit vector along the direction of $\mathbf{B}_0$, and $\hat{\mathbf{x}}$ and $\hat{\mathbf{z}}$ are unit vectors in the x and z directions, respectively.

Then, using (4) in (1) and making some algebraic operations combined with Equations (2) and (3), we can obtain the expression for $\bar{\varepsilon}_m$, that is

$$\bar{\varepsilon}_m = \begin{bmatrix} \varepsilon_{xx,m} & \varepsilon_{xy,m} & \varepsilon_{xz,m} \\ \varepsilon_{yx,m} & \varepsilon_{yy,m} & \varepsilon_{yz,m} \\ \varepsilon_{zx,m} & \varepsilon_{zy,m} & \varepsilon_{zz,m} \end{bmatrix} \tag{5}$$

The components $\varepsilon_{ij,m}$ $(i, j = x, y, z)$ of (5) are as follows

$$\begin{cases} \varepsilon_{xx,m} = \varepsilon_0 + K\left(U^2 + N^2\right),\ \varepsilon_{xy,m} = -KUM,\ \varepsilon_{xz,m} = KMN; \\ \varepsilon_{yx,m} = -\varepsilon_{xy,m},\ \varepsilon_{yy,m} = \varepsilon_0 + KU^2,\ \varepsilon_{yz,m} = -KUN; \\ \varepsilon_{zx,m} = \varepsilon_{xz,m},\ \varepsilon_{zy,m} = -\varepsilon_{yz,m},\ \varepsilon_{zz,m} = \varepsilon_0 + K\left(U^2 + M^2\right); \\ U = j\omega + \nu_{en},\ M = \omega_b \cos\theta_B,\ N = \omega_b \sin\theta_B,\ K = \frac{\varepsilon_0 \omega_{p,m}^2}{j\omega U\left(U^2 + \omega_b^2\right)}; \end{cases} \tag{6}$$

Therefore, given that the plasma parameters across the whole slab are known, the permittivity characteristics of the proposed EM problem model can be gained by above methods.

2.2. The State Vector and Eigen Waves in Anisotropic, Layered Media

In this part, the state vector is used to describe the characteristics of the eigen waves for the EM problem model shown in Figure 1. It is known that there are two kinds of eigen wave in an anisotropic media such as magnetized plasma [20], one is called type I wave and the other is type II wave. These two types of waves are coupled to each other at the interface — in other words, a type I wave may produce transmitted and reflected waves of both type I and type II. Considering the general case that the permittivity and the permeability of an anisotropic media are tensors, the Maxwell's equations for source-free, anisotropic media are [28]:

$$\nabla \times \mathbf{E} = -j\omega\bar{\mu} \cdot \mathbf{H} \tag{7a}$$

$$\nabla \times \mathbf{H} = j\omega\bar{\varepsilon} \cdot \mathbf{E} \tag{7b}$$

When the electromagnetic properties of the anisotropic medium, the permittivity $\bar{\varepsilon}$ and the permeability $\bar{\mu}$, are varying only in the z

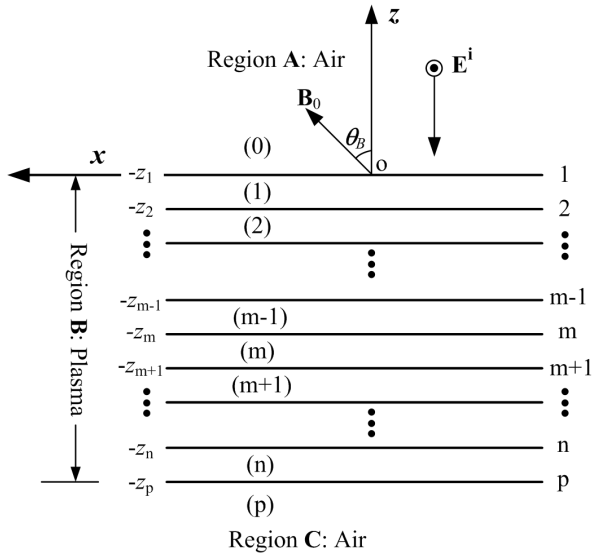

Figure 1. The EM problem model of a plane wave normally incident on a nonuniform magnetized plasma slab with arbitrary magnetic field declination ($z_1 = 0$, $z_i > 0$, $i = 2, 3, \ldots, n, p$).

direction, it is expedient to decompose $\nabla = \nabla_s + \hat{z}\frac{\partial}{\partial z}$, $\mathbf{E} = \mathbf{E}_s + \mathbf{E}_z$, $\mathbf{H} = \mathbf{H}_s + \mathbf{H}_z$, and $\bar{\varepsilon}$ and $\bar{\mu}$ can be partitioned as

$$\bar{\varepsilon} = \begin{bmatrix} \bar{\varepsilon}_s & \bar{\varepsilon}_{sz} \\ \bar{\varepsilon}_{zs} & \bar{\varepsilon}_{zz} \end{bmatrix}, \quad \bar{\mu} = \begin{bmatrix} \bar{\mu}_s & \bar{\mu}_{sz} \\ \bar{\mu}_{zs} & \bar{\mu}_{zz} \end{bmatrix} \tag{8}$$

where the subscript s denotes qualities transverse to z axis. In the forms mentioned above, $\bar{\varepsilon}_s$ is a 2×2 tensor, $\bar{\varepsilon}_{sz}$ is a 2×1 matrix, $\bar{\varepsilon}_{zs}$ is a 1×2 matrix, and $\bar{\varepsilon}_{zz}$ is a 1×1 matrix. Similar decomposition holds for $\bar{\mu}$. Furthermore, considering phase matching, we assume that the fields $\mathbf{E}_s$ and $\mathbf{H}_s$ have $e^{jk_s \cdot r_s}$ ($\mathbf{k}_s$ is a propagation vector transverse to the z direction) dependence in the transverse direction for all z's. By substituting the decomposition into (7) and crossing with $\hat{\mathbf{z}}$ on both sides, after making some algebraic operations, we get:

$$\frac{d}{dz}\mathbf{E}_s = \left[(j\omega\hat{\mathbf{z}}\times\bar{\mu}_s\cdot) - j\omega\hat{\mathbf{z}}\times\bar{\mu}_{sz}\cdot\bar{\mu}_{zs}\cdot v_{zz} + \left(\frac{j\hat{\mathbf{z}}}{\omega}\times\mathbf{k}_s\times k_{zz}\mathbf{k}_s\times\right)\right]\mathbf{H}_s + \left[(j\hat{\mathbf{z}}\times\bar{\mu}_{sz}\cdot v_{zz}\mathbf{k}_s\times) + j\hat{\mathbf{z}}\times\mathbf{k}_s\times k_{zz}\bar{\varepsilon}_{zs}\cdot\right]\mathbf{E}_s \tag{9a}$$

$$\frac{d}{dz}\mathbf{H}_s = \left[(-j\omega\hat{\mathbf{z}}\times\bar{\varepsilon}_s\cdot) + j\omega\hat{\mathbf{z}}\times\bar{\varepsilon}_{sz}\cdot\bar{\varepsilon}_{zs}\cdot k_{zz} - \left(\frac{j\hat{\mathbf{z}}}{\omega}\times\mathbf{k}_s\times v_{zz}\mathbf{k}_s\times\right)\right]\mathbf{E}_s + \left[(j\hat{\mathbf{z}}\times\bar{\varepsilon}_{sz}\cdot k_{zz}\mathbf{k}_s\times) + j\hat{\mathbf{z}}\times\mathbf{k}_s\times v_{zz}\bar{\mu}_{zs}\cdot\right]\mathbf{H}_s \tag{9b}$$

where $k_{zz} = \varepsilon_{zz}^{-1}$, $v_{zz} = \mu_{zz}^{-1}$, and ∇_s has been replaced by $-j\mathbf{k}_s$.

The preceding Equations (9a) and (9b) can be expressed in a matrix form as a state equation

$$\frac{d}{dz}\mathbf{V} = \bar{\mathbf{C}} \cdot \mathbf{V} \tag{10}$$

where $\bar{\mathbf{C}}$ is a 4×4 matrix called as eigenmatrix, $\mathbf{V}^t = [\mathbf{E}_s \ \mathbf{H}_s]^t = [E_x \ E_y \ H_x \ H_y]^t$ (the superscript t denotes transpose of a matrix) is the state vector describing the state of the system. The explicit expressions for the components c_{ij} (i, $j = 1, 2, 3, 4$) of $\bar{\mathbf{C}}$ can be derived from (9a) and (9b).

For the entire EM problem space depicted in Figure 1, $\bar{\mu}$ is reduced to $\mu_0\mathbf{I}$ (μ_0 is the permeability in vacuum), and we have $\mathbf{k}_s = 0$ due to the normal incidence of the plane wave, so the eigenmatrix $\bar{\mathbf{C}}$ for any one region can be simplified greatly. Taking the m-th layer of plasma slab in Region **B** for example, the components $c_{ij,m}$ for that layer can be obtained by using (5) and (6) in (9) and (10), which are shown as follows:

$$\begin{cases} c_{11,m} = 0, \ c_{12,m} = 0, \ c_{13,m} = 0, \ c_{14,m} = -j\omega\mu_0; \\ c_{21,m} = 0, \ c_{22,m} = 0, \ c_{23,m} = j\omega\mu_0, \ c_{24,m} = 0; \\ c_{31,m} = j\left(\omega\varepsilon_{yx,m} - \frac{\omega\varepsilon_{yz,m}\varepsilon_{zx,m}}{\varepsilon_{zz,m}}\right), \ c_{32,m} = j\left(\omega\varepsilon_{yy,m} - \frac{\omega\varepsilon_{yz,m}\varepsilon_{zy,m}}{\varepsilon_{zz,m}}\right); \\ c_{33,m} = 0, \ c_{34,m} = 0; \\ c_{41,m} = j\left(-\omega\varepsilon_{xx,m} + \frac{\omega\varepsilon_{xz,m}\varepsilon_{zx,m}}{\varepsilon_{zz,m}}\right), \ c_{42,m} = j\left(-\omega\varepsilon_{xy,m} + \frac{\omega\varepsilon_{xz,m}\varepsilon_{zy,m}}{\varepsilon_{zz,m}}\right); \\ c_{43,m} = 0, \ c_{44,m} = 0 \end{cases} \tag{11}$$

where the components c_{ij} of $\bar{\mathbf{C}}$ for the m-th layer are denoted as $c_{ij,m}$ for convenience. As for Region **A** and Region **C**, $\bar{\varepsilon}$ is also reduced to $\varepsilon_0\mathbf{I}$, and the eigenmatrix $\bar{\mathbf{C}}$ of these spaces will be more simple, which can be inferred from (11) through replacing $\bar{\varepsilon}_m$ by $\varepsilon_0\mathbf{I}$.

By letting $\mathbf{V} = \mathbf{V}_0 e^{\lambda z}$ and making use of it in (10), the state equation can be converted to an eigenequation for the eigenvalue λ. That is

$$\left(\bar{\mathbf{C}} - \lambda\bar{I}\right) \cdot \mathbf{V}_0 = 0 \tag{12}$$

Therefore, given that the eigenmatrix $\bar{\mathbf{C}}$ for any one region shown in Figure 1 is specified, the general solution to (10), viz., the state vector of that region, can be found through elementary transformation of (12) [29], which is shown as the following form

$$\mathbf{V}(z) = B_1\mathbf{a}_1 e^{-j\beta_1 z} + B_2\mathbf{a}_2 e^{-j\beta_2 z} + B_3\mathbf{a}_3 e^{j\beta_3 z} + B_4\mathbf{a}_4 e^{j\beta_4 z} = \bar{\mathbf{a}} \cdot e^{j\bar{\beta}z} \cdot \mathbf{B} \tag{13}$$

where $\bar{\mathbf{a}}$ is a 4×4 matrix containing the column vectors $\mathbf{a}_i$'s, i.e., $\bar{\mathbf{a}} = [\mathbf{a}_1, \mathbf{a}_2, \mathbf{a}_3, \mathbf{a}_4]$, and $\mathbf{a}_i$ is the eigenvector corresponding to the i-th eigenvalue of the matrix $\bar{\mathbf{C}}$. **B** is a four-component column vector

containing B_i's which represent the amplitudes of type I and type II waves going in the positive and negative z directions. Moreover, $j\bar{\beta}(= \text{diag}(-j\beta_1 \; -j\beta_2 \, j\beta_3 \, j\beta_4))$ is a diagonal matrix where the i-th diagonal element corresponds to the i-th eigenvalue. According to the definition of the exponentiation of a matrix, $e^{j\bar{\beta}z}$ can be written as

$$e^{j\bar{\beta}z} = \begin{bmatrix} e^{-j\beta_1 z} & & & \\ & e^{-j\beta_2 z} & & \\ & & e^{j\beta_3 z} & \\ & & & e^{j\beta_4 z} \end{bmatrix} \tag{14}$$

In the above, these eigenvalues and eigenvectors are ordered such that the first two elements of (14) correspond to type I and type II waves going in the positive z direction while the last two elements correspond to the downgoing ones traveling in the negative z direction.

Considering the physical mechanism of EM waves propagating in anisotropic magnetized plasma [30], it is easy to find that $\beta_1 = \beta_3$, $\beta_2 = \beta_4$, and β_1 (or β_3) corresponds to the z-component of propagation constants of type I wave while β_2 (or β_4) corresponds to the one of type II wave. As for isotropic medium such as the un-magnetized plasma or the air in Region **A** and Region **C**, all the β_i ($i = 1, 2, 3, 4$) of the state vector have the same values and type I and type II waves are reduced to TE (field components are E_y and H_x) and TM (field components are E_x and H_y) waves in this case.

2.3. Formulae for Calculating the Propagation and Polarization Properties of the Proposed EM Problem Model

Noting the fact $\bar{\mathbf{a}}^{-1} \cdot \bar{\mathbf{a}} = \bar{\mathbf{I}}$, (13) can be rewritten as

$$\mathbf{V}(z) = \bar{\mathbf{a}} \cdot e^{j\bar{\beta}(z-z')} \cdot \bar{\mathbf{a}}^{-1} \cdot \bar{\mathbf{a}} \cdot e^{j\bar{\beta}z'} \cdot \mathbf{B} = \bar{\mathbf{P}}\left(z, z'\right) \cdot \mathbf{V}(z') \tag{15}$$

where

$$\bar{\mathbf{P}}\left(z, z'\right) = \bar{\mathbf{a}} \cdot e^{j\bar{\beta}(z-z')} \cdot \bar{\mathbf{a}}^{-1} \tag{16}$$

The matrix $\bar{\mathbf{P}}$ is known as the propagator matrix which relates the state vectors that describe the fields at two different locations z and z' in one region.

Since the elements of the state vector $\mathbf{V}(z)$ (related to the tangential components of the electric and magnetic fields) are continuous quantities across an interface, the $\bar{\mathbf{P}}$ matrix for the total plasma region, i.e., Region **B** shown in Figure 1, would just be the product of the $\bar{\mathbf{P}}$ matrix of each of the layers. Denoting the state vector of Region $\mathbf{X}$ ($\mathbf{X} = \mathbf{A}, \mathbf{B}, \mathbf{C}$) shown in Figure 1 as $\mathbf{V}_X(z)$, the $\bar{\mathbf{P}}$

matrix can be used to find $\mathbf{V}_C(-z_p)$ in terms of $\mathbf{V}_A(0)$, that is

$$\begin{aligned}\mathbf{V}_C(z=-z_p) &= \mathbf{V}_B(-z_p) = \bar{\mathbf{P}}(-z_p,-z_n)\cdot\mathbf{V}_B(-z_n)\\ &= \bar{\mathbf{P}}(-z_p,-z_n)\cdot\bar{\mathbf{P}}(-z_n,-z_{n-1})\cdot\mathbf{V}_B(-z_{n-1})\\ &= \left[\prod_{i=n}^{1}\bar{\mathbf{P}}(-z_{i+1},-z_i)\right]\cdot\mathbf{V}_B(0) = \bar{\mathbf{P}}_B(-z_p,0)\cdot\mathbf{V}_B(0)\\ &= \bar{\mathbf{P}}_B(-z_p,0)\cdot\mathbf{V}_A(0) \qquad (17)\end{aligned}$$

where $z_{n+1}=z_p$, $z_1=0$ and $\bar{\mathbf{P}}_B(-z_p,0)=[\prod_{i=n}^{1}\bar{\mathbf{P}}(-z_{i+1},-z_i)]$. The matrix $\bar{\mathbf{P}}_B$ can be referred to as the global propagator matrix which gives the relation between the state vector of the 0-th layer (above the slab, into which the reflected wave is returned) and the p-th layer (below the slab, into which the transmitted wave is propagating).

Note that our goal is to gain the propagation and polarization characteristics of EM waves interaction with the nonuniform magnetized plasma slab as sketched in Figure 1, hence, a reflection matrix $\bar{\mathbf{R}}$ and a transmission matrix $\bar{\mathbf{T}}$ are defined as

$$\begin{bmatrix} B_{1A}\\ B_{2A}\end{bmatrix} = \bar{\mathbf{R}}\cdot\begin{bmatrix} B_{3A}\\ B_{4A}\end{bmatrix}, \quad \begin{bmatrix} B_{3C}\\ B_{4C}\end{bmatrix} = \bar{\mathbf{T}}\cdot\begin{bmatrix} B_{3A}\\ B_{4A}\end{bmatrix} \qquad (18a)$$

$$\bar{\mathbf{R}} = \begin{bmatrix} R_{11} & R_{12}\\ R_{21} & R_{22}\end{bmatrix}, \quad \bar{\mathbf{T}} = \begin{bmatrix} T_{11} & T_{12}\\ T_{21} & T_{22}\end{bmatrix} \qquad (18b)$$

where B_{1A} and B_{2A} are the amplitudes of the upgoing TE and TM waves in Region **A**, while B_{3A} (B_{3C}) and B_{4A} (B_{4C}) are the amplitudes of the downgoing TE and TM waves in Region **A** (**C**), respectively. Here, B_{3A} and B_{4A}, the downgoing or incident wave amplitudes, are assumed to be known, and $\bar{\mathbf{R}}$ and $\bar{\mathbf{T}}$ are the unknowns to be sought in this problem.

Using (13) and (18), the state vector in Region **A** can be expressed as

$$\mathbf{V}_A(z) = \bar{\mathbf{a}}_A\cdot e^{j\bar{\beta}_A z}\cdot\begin{bmatrix}\bar{\mathbf{R}}\\ \bar{\mathbf{I}}\end{bmatrix}\cdot\begin{bmatrix} B_{3A}\\ B_{4A}\end{bmatrix} \qquad (19)$$

where the subscript A is used to denote that Equation (19) is for the solution in Region **A**. In Region **C**, only downgoing waves exist. Similarly, the $\bar{\mathbf{T}}$ can be used to express the state vector in Region **C** as

$$\mathbf{V}_C(z) = \bar{\mathbf{a}}_C\cdot e^{j\bar{\beta}_C(z+z_p)}\cdot\begin{bmatrix}0\\ \bar{\mathbf{T}}\end{bmatrix}\cdot\begin{bmatrix} B_{3A}\\ B_{4A}\end{bmatrix} \qquad (20)$$

Substituting (19) and (20) into (17), we conclude that

$$\bar{\mathbf{a}}_C^{-1}\cdot\bar{\mathbf{P}}_B(-z_p,0)\cdot\bar{\mathbf{a}}_A\cdot\begin{bmatrix}\bar{\mathbf{R}}\\ \bar{\mathbf{I}}\end{bmatrix} = \begin{bmatrix}0\\ \bar{\mathbf{T}}\end{bmatrix} \qquad (21)$$

Given that the plasma parameters of the whole slab shown in Figure 1 are known, we can obtain the state vector and the propagator matrix for each region of the proposed EM problem model, and then $\bar{\mathbf{R}}$ and $\bar{\mathbf{T}}$ can be got easily through solving (21).

Moreover, the four elements of $\bar{\mathbf{R}}$ ($\bar{\mathbf{T}}$) present the coupling relations of the reflected (transmitted) TE and TM waves, which demonstrates a phenomenon of the transformation of wave polarization. In other words, a y-polarized wave incident on the magnetized plasma slab may produce two reflected and transmitted waves. One is y-polarized wave standing for co-polarized wave, and the other is x-polarized wave indicated as cross-polarized wave. For the problem considered here, R_{21} (T_{21}) reveals the reflection (transmission) coefficient for the case that the incident plane wave is TE wave but the generated reflection (transmission) wave is TM wave, while R_{11} (T_{11}) represents the reflection (transmission) coefficient for the case that the incident wave and the produced reflection (transmission) wave are both TE waves. Therefore, R_{21} (T_{21}) can be referred to as the reflection (transmission) coefficient of cross-polarization, and R_{11} (T_{11}) can be suggested as the reflection (transmission) coefficient of co-polarization. Other elements of $\bar{\mathbf{R}}$ ($\bar{\mathbf{T}}$) also have similar signification which can be easily deduced from above and will not be discussed here.

Therefore, when the plane wave with electric vector polarized in the y direction (i.e., TE wave) is incident normally on the nonuniform magnetized slab as depicted in Figure 1, the normalized reflected and transmitted powers of co-polarization and cross-polarization are, respectively, given by:

$$\text{normalized reflected power of co-polarization: } P_{r\_\text{co}} = |R_{11}|^2 \tag{22a}$$

$$\text{normalized reflected power of cross-polarization: } P_{r\_\text{cross}} = |R_{21}|^2 \tag{22b}$$

$$\text{normalized transmitted power of co-polarization: } P_{t\_\text{co}} = |T_{11}|^2 \tag{22c}$$

$$\text{normalized transmitted power of cross-polarization: } P_{t\_\text{cross}} = |T_{21}|^2 \tag{22d}$$

As for un-magnetized plasma slab, the reflected and transmitted powers of cross-polarization vanish due to the isotropic property of the medium.

The normalized absorbed power of TE wave through the plasma slab can be easily obtained after knowing total reflection and transmission powers, which is given as

$$P_a = 1 - P_{r\_\text{co}} - P_{r\_\text{cross}} - P_{t\_\text{co}} - P_{t\_\text{cross}} \tag{22e}$$

The absorbed power P_a in (22e) is derived from the EM kinetic theory for plasma, so the physical mechanism responsible for the absorption contains the collisional damping as well as the Landau damping, both

of which contribute to the exchange of energy between waves and particles.

3. NUMERICAL VERIFICATION AND RESULTS ANALYSIS

3.1. Validity Analysis

In order to check the validity of the proposed propagator matrix method (PMM), a test is done by considering a uniform magnetized plasma plate which is similar to the case studied by Yin et al. [20]. Here, the plate parameters are selected as: $\omega_p = 2\pi \times 28.7 \times 10^9$ rad/s, $\omega_b = 8.8 \times 10^{10}$ rad/s, $\nu_{en} = 2 \times 10^{10}$ rad/s and the plate thickness is 9 mm. A plane wave is assumed to be incident normally on the plate with its wave vector perpendicular to external magnetic field $\mathbf{B}_0$. It is known that there are two kinds of eigen waves in this case. One is ordinary wave (O-wave), and the other is extraordinary wave (X-wave) [30]. Subsequently, three methods, i.e., the PMM proposed in this paper, the analytical method and the SO-FDTD method introduced in [20], are used to calculate EM wave propagating through this plate. When PMM is used, note that O-wave and X-wave are linearly polarized waves and not coupled with each other, the reflection and transmission coefficients of X-wave (O-wave) can be obtained by R_{11} (R_{22}) and T_{11} (T_{22}), respectively. As for the application of the SO-FDTD method, the settings for calculation are the same as those

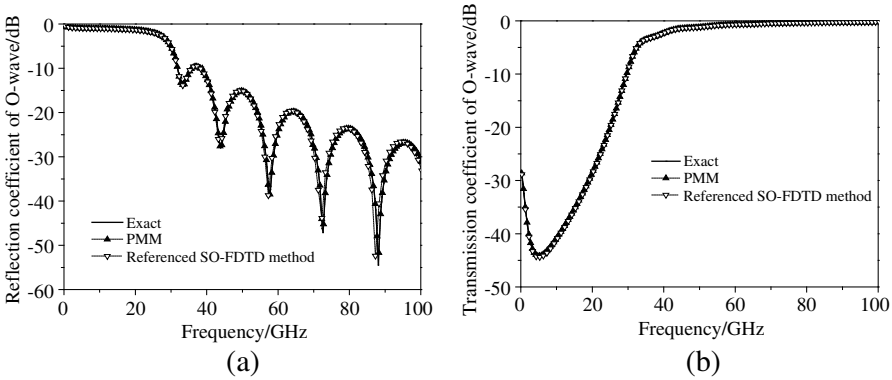

Figure 2. O-wave reflection and transmission coefficients against frequency for a plasma plate magnetized by a background magnetic field perpendicular to the wave propagation direction. (a) Reflection coefficient magnitude. (b) Transmission coefficient magnitude.

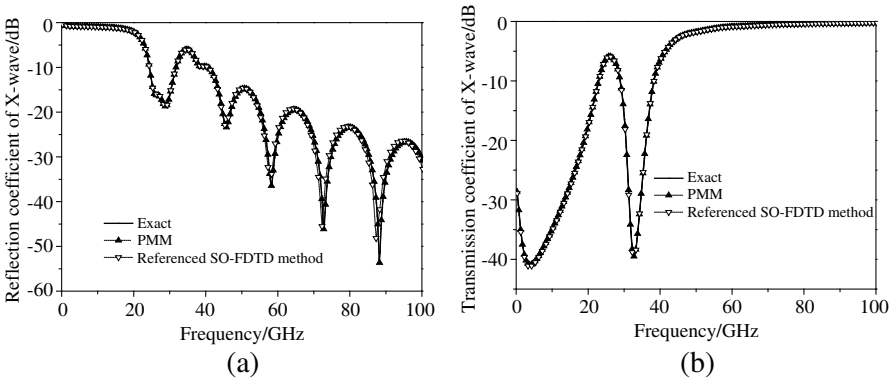

Figure 3. X-wave reflection and transmission coefficients against frequency for a plasma plate magnetized by a background magnetic field perpendicular to the wave propagation direction. (a) Reflection coefficient magnitude. (b) Transmission coefficient magnitude.

Table 1. Comparison of the average running times used for PMM and the referenced SO-FDTD method proposed in [20]. (Each program was allowed to run for ten times to obtain an average time cost.).

	PMM	referenced SO-FDTD
CPU time, s	0.395083 s	1.683555 s

in [20] except for the parameters of plasma. Moreover, the magnetic declination angles θ_B are set as 90° for both PMM and the SO-FDTD method.

The reflection and transmission coefficients of O-wave and X-wave calculated by three methods are shown in Figures 2 and 3, respectively. From these figures, it is found that the results of PMM coincide with the analytical method very well over the entire frequency band and are more accurate than the SO-FDTD method, which can be easily seen from Figures 2(a) and 3(a) where the SO-FDTD solution strays a bit from the analytical solution when the incident wave frequency is sufficiently high. Moreover, the time cost of calculating by a computer based on Intel(R) Core(TM) i5-2400 CPU @ 3.10 GHz using the PMM and the SO-FDTD method is summarized in Table 1. It should be noticed that the programs of the two methods had been carried out for ten times to gain the average time cost. These data of Table 1 show that the machine time of PMM is much less than that of the referenced FDTD method, indicating that the former is more efficient than the numerical FDTD method due to a great reduction of memory

resources. The test confirmed the high efficiency and accuracy of the PMM proposed in this paper.

3.2. The Electron Density Distribution for the Proposed Magnetized Plasma Slab

Now, a certain density profile for the proposed magnetized plasma slab is presented. From a physical perspective, the electron density should follow the distribution that it goes to zero near the plasma-air interface and reaches the maximum in a limited distance from one interface, which have been validated and adopted by many researchers [2, 3, 10–12, 14, 15, 17]. The experiments about the plasma sheath [10, 11] show that the electron density profile for plasma objects may follow a bi-exponential curve. Therefore, the bi-exponential function distribution will be adopted for our EM problem model, which can be expressed as

$$n_e(z) = \begin{cases} N_{e0} e^{-\frac{z+L_1}{z_{10}}} & -L_1 \le z \le 0 \\ N_{e0} e^{\frac{z+L_1}{z_{20}}} & -L_2 \le z \le -L_1 \end{cases} \tag{23}$$

In the above, z is the radial distance, N_{e0} is the peak of electron density, z_{10} and z_{20} represents the curve's shape, L_1 determines the location where electron density reaches the maximum, and L_2 specifies the thickness of the plasma. In the following simulation, some parameters of (23) are designated as constants, which are: $L_1 = 15\,\text{cm}$, $L_2 = 60\,\text{cm}$ (that is to say, the thickness of the plasma slab is 60 cm), $z_{10} = 1\,\text{cm}$, $z_{20} = 4\,\text{cm}$. Furthermore, it is assumed that the collision frequency and the cyclotron frequency are identical for all layers of the nonuniform plasma slab shown in Figure 1, and the slab is divided into 1600 uniform layers each of which has fixed electron density. The overall density profile follows the bi-exponential function mentioned above. This multi-layers treatment has been proved to be good enough for representing the nonuniform nature of the density profile.

3.3. Propagation and Polarization Characteristics Affected by Electron Density

We consider various electron density distribution under different N_{e0}. It is known that the relationship between the plasma frequency f_p and the electron density n_e can be expressed as [30]

$$f_p = \frac{\omega_p}{2\pi} = \frac{1}{2\pi}\left(\frac{n_e e^2}{\varepsilon_0 m_e}\right)^{1/2} \tag{24}$$

where e is the electron charge and m_e the mass of an electron. Figure 4 shows the plasma frequency distribution as a function of

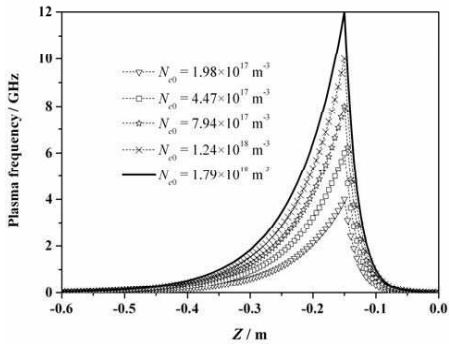

Figure 4. Relationship between the plasma thickness and the plasma frequency for the bi-exponential electron density profile with different N_{e0}.

plasma thickness with different N_{e0} calculated using (23) and (24). (The peak density N_{e0} are given respectively by $1.98 \times 10^{17}\,\mathrm{m}^{-3}$, $4.47 \times 10^{17}\,\mathrm{m}^{-3}$, $7.94 \times 10^{17}\,\mathrm{m}^{-3}$, $1.24 \times 10^{18}\,\mathrm{m}^{-3}$, $1.79 \times 10^{18}\,\mathrm{m}^{-3}$, and thus the maximum plasma frequencies are 4 GHz, 6 GHz, 8 GHz, 10 GHz and 12 GHz according to Equation (24)). It is shown in Figure 4 that the variance of plasma frequency with the radial distance becomes faster as N_{e0} is bigger.

When the magnetic declination angle θ_B is set as 45°, the collision frequency ν_{en}, 1 GHz, and the electron cyclotron frequency ω_b, $2\pi \times 2 \times 10^9$ rad/s, the effects of different peak density N_{e0} on the reflected and transmitted powers of co-polarization and cross-polarization, as well as the absorbed power are calculated with PMM and shown in Figure 5.

It is apparent in Figure 5(a) that the incidence frequency range of 1–19 GHz can be distinguished by a turning frequency point which approximately is equal to the cyclotron frequency $f_b = \omega_b/2\pi = 2$ GHz. The reflected power of co-polarization P_{r_co} comes to the minimum at this point. For convenience of description, these turning points are denoted as f_t uniformly. Within the frequency band of 1 GHz-f_t, there is no effect of density N_{e0} on P_{r_co}, and P_{r_co} reduces quickly as the incidence frequency increases and even reach the minimum value at f_t. When wave frequency exceeds f_t, the electron density distribution affects P_{r_co} sharply. As the frequency goes from f_t to 19 GHz, P_{r_co} becomes larger until it goes to a maximum value, and then decreases gradually even approaching zero. Generally, the maximum value of P_{r_co} and the corresponding incidence frequency increase with rise of density N_{e0}, but when N_{e0} overruns $1.24 \times 10^{18}\,\mathrm{m}^{-3}$, the maximum value of P_{r_co} has almost no changes. While for the normalized reflected

power of cross-polarization P_{r_cross} as shown in Figure 5(b), there are two troughs and two peaks within the entire frequency band. The first trough appears at the frequency of about 1.9 GHz which approximates to f_b, and the frequency of the second one increases from 2.95 to 3.55 GHz as the density N_{e0} increases from $1.98 \times 10^{17}\,\text{m}^{-3}$ to $1.79 \times 10^{18}\,\text{m}^{-3}$. The first peak occurs around 2.35 GHz, and the magnitude of it is much less than that of the second peak and is less affected by the density N_{e0}. The second peak appears around the maximum plasma frequency $f_{p,\max}$, and the magnitude of it increases with the increase of density N_{e0}. Furthermore, Figures 5(a) and (b) demonstrate that the comparatively larger values for P_{r_co} and P_{r_cross} can be obtained within most of frequency ranges with a bigger density N_{e0}, since increasing the electron density forces the plasma to behave like a perfect conductor.

Figure 5(c) indicates that there is a turning change for transmitted power of co-polarization P_{t_co} around the corresponding maximum plasma frequency $f_{p,\max}$ (i.e., $f_{p,\max}$ also can be seen as the turning point in this case). On the precondition of a fixed density N_{e0}, it is easy

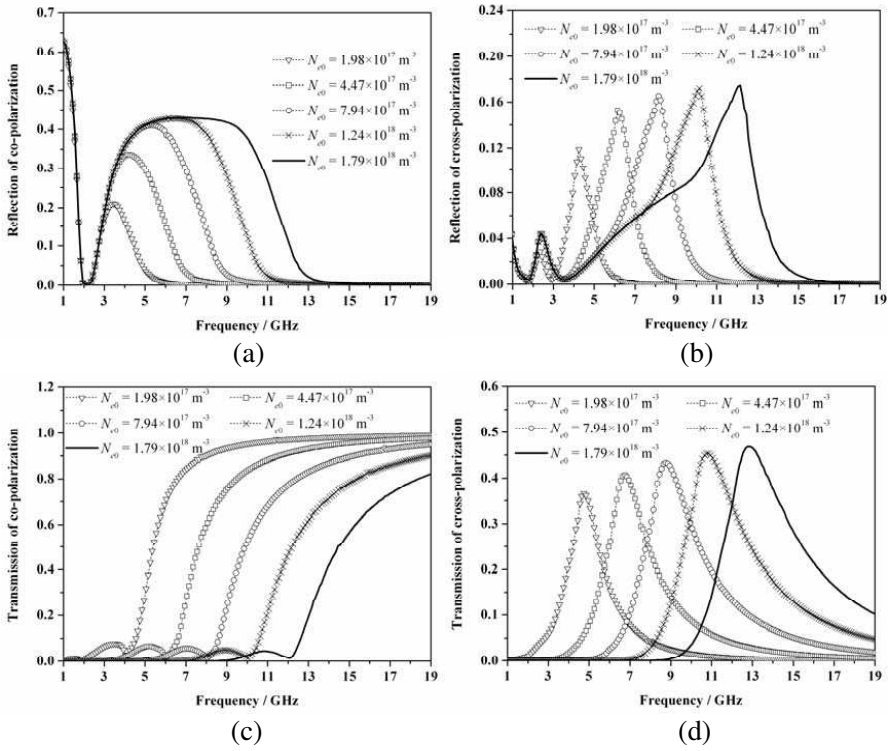

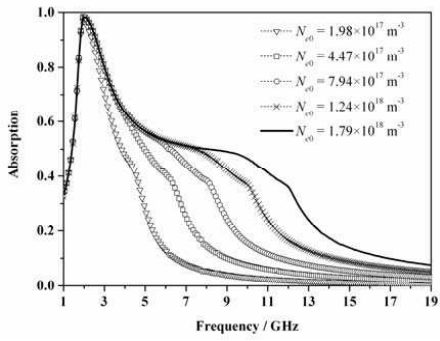

(e)

Figure 5. Normalized power versus wave frequency for different peak electron density. (a) Normalized reflected power of co-polarization: P_{r_co}. (b) Normalized reflected power of cross-polarization: P_{r_cross}. (c) Normalized transmitted power of co-polarization: P_{t_co}. (d) Normalized transmitted power of cross-polarization: P_{t_cross}. (e) Normalized absorbed power: P_a.

to find that P_{t_co} increases slowly at first and then reduces gradually, which shows a small peak value, as incidence frequency increases from 1 GHz to $f_{p,\max}$. When the frequency exceeds $f_{p,\max}$, P_{t_co} increases rapidly and then goes to 1 gently. This phenomenon can be explained that when the incidence EM wave frequency is lower than the maximum plasma frequency, the EM wave will be completely reflected in the progress of incidence, and only such EM wave whose frequency is higher than maximum plasma frequency could transport through plasma layers. On the other hand, when the incidence frequency varies from the turning point $f_{p,\max}$ to 19 GHz, the smaller the density N_{e0} is, the more quickly P_{t_co} grows up toward 1, and the greater P_{t_co} can be gained at the same frequency.

As shown in Figure 5(d), for transmitted power of cross-polarization P_{t_cross} with a stable value N_{e0}, there exists an optimum incidence frequency at which the P_{t_cross} reaches a maximum value. When incidence frequency is smaller than the optimum incidence frequency, the bigger incidence frequency is, the higher P_{t_cross} has. Otherwise, the bigger incidence frequency is, the less P_{t_cross} has. Moreover, the maximum value and the corresponding optimum incidence frequency increases with increasing the density N_{e0}. Compared to the results drawn in Figure 5(c), it is easy to find that P_{t_co} is rather small at this optimum frequency.

It is seen from Figure 5(e) that, with a certain density N_{e0}, the absorbed power P_a firstly increases to a maximum value at

the frequency equaling to f_b and then reduces gradually, as the incidence frequency increases. Though there is almost no effect of different density N_{e0} on the maximum value of P_a, the absorption band becomes wider as the density N_{e0} increases. The reason why P_a has a maximum at the frequency equaling to f_b is that when the incidence frequency matches the cyclotron frequency, it generates electron circular resonance (ECR) absorption, which converts the wave energy into the kinetic energy of the plasma particles intensely.

3.4. Propagation and Polarization Characteristics Affected by Collision Frequency

The reflected and transmitted powers of co-polarization and cross-polarization as well as the absorbed power with different collision frequency are calculated and described in Figure 6, where the density N_{e0} is set to $7.94 \times 10^{17}\,\mathrm{m}^{-3}$ (corresponding to the maximum plasma frequency 8 GHz), the magnetic declination angle θ_B, 45°, and the cyclotron angular frequency ω_b, $2\pi \times 2 \times 10^9\,\mathrm{rad/s}$. It is clear from Figure 6 that, under different collision frequency, the reflected,

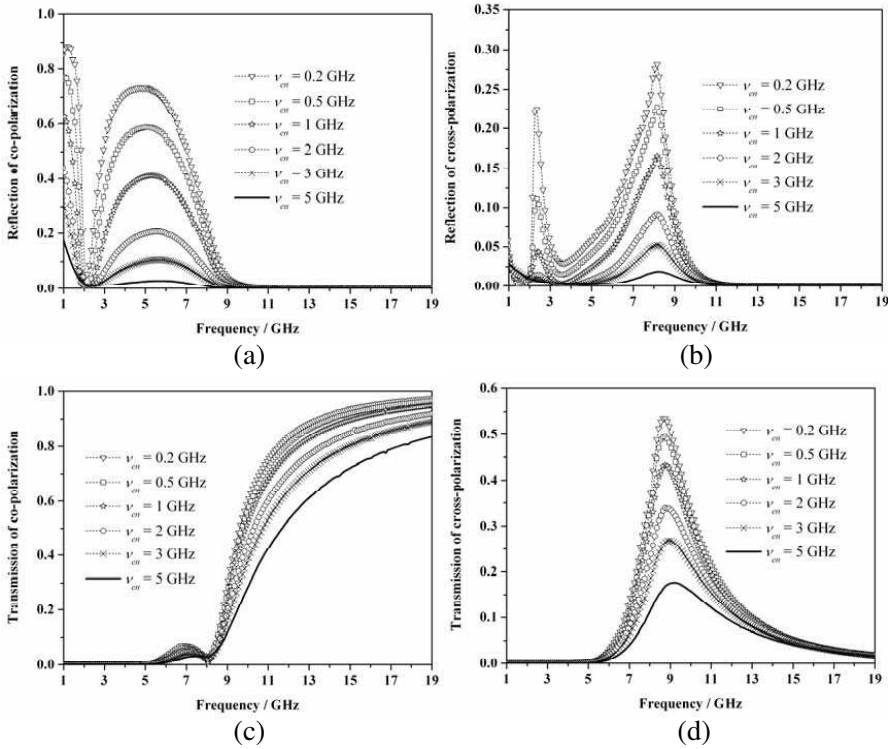

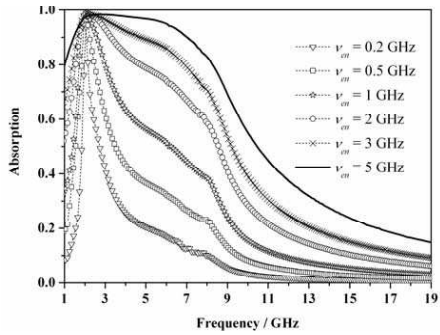

(e)

Figure 6. Normalized power versus wave frequency for different collision frequency. (a) Normalized reflected power of co-polarization: P_{r_co}. (b) Normalized reflected power of cross-polarization: P_{r_cross}. (c) Normalized transmitted power of co-polarization: P_{t_co}. (d) Normalized transmitted power of cross-polarization: P_{t_cross}. (e) Normalized absorbed power: P_a.

transmitted and absorbed powers have same variation trends with rise of frequency, respectively. But there exist great differences between these peak values.

Figures 6(a), (b), (c) and (d) show that within most of the frequency ranges, the lower the collision frequency is, the larger P_{r_co}, P_{r_cross}, P_{t_co} and P_{t_cross} are at the same incidence frequency. This phenomenon is expected because the process of reflection or transmission is accompanied by significant absorption of wave energy caused by intense collisions which transfer momentum between EM waves and the particles. Moreover, P_{r_co}, P_{r_cross}, P_{t_co} and P_{t_cross} present a variation regularity similar to that shown in Figures 5(a), (b), (c) and (d), respectively, except the fact that different collision frequency ν_{en} does not cause visible frequency position variation of the extreme values especially for the minimum values. As to the same extreme value, the maximum value is greater with a comparatively smaller ν_{en}.

As shown in Figure 6(e), the absorbed power P_a also approaches to the maximum when the frequency is close to the cyclotron frequency, and the plasma with a higher collision frequency has a wider absorption bandwidth, because the plasma will absorb more energy from EM wave when the effective collision frequency becomes higher. On the other hand, there is almost no effect on the maximum value of the absorbed power when the collision frequency increases from 0.2 GHz to 5 GHz.

3.5. Propagation and Polarization Characteristics Affected by Cyclotron Frequency

Figure 7 shows P_{r_co}, P_{r_cross}, P_{t_co}, P_{t_cross} and P_a versus the incidence frequency for different cyclotron frequency f_b, respectively. Some plasma parameters are the density $N_{e0} = 7.94\times10^{17}\,\mathrm{m}^{-3}$, the magnetic declination angle $\theta_B = 45^\circ$ and the collision frequency $\nu_{en} = 1\,\mathrm{GHz}$. It is seen from Figures 7(a) and (b) that the effects of cyclotron frequency on reflected powers of co-polarization and cross-polarization are complicated. In general, there also exists a frequency band around the cyclotron frequency where P_{r_co} and P_{r_cross} reach rather small values. Moreover, there are more ripples in the curves of P_{r_co} and P_{r_cross}, and the curvy fluctuations vary more sharply, as the cyclotron frequency increases. Within the low frequency band (e.g., 1–4 GHz), the larger the cyclotron frequency is, the bigger P_{r_cross} can be obtained. However, the regularities about the relationship between P_{r_cross} and the cyclotron frequency are not clear over other frequency ranges. The P_{r_co} variation regularity with the cyclotron frequency seems to be fuzzy within most of the frequency band. The behavior of

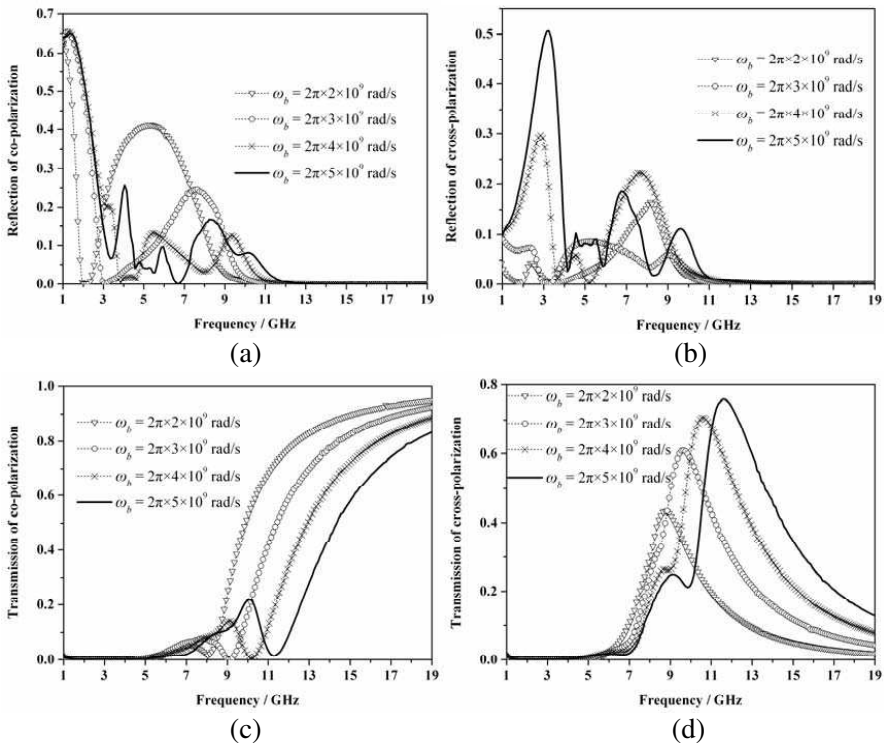

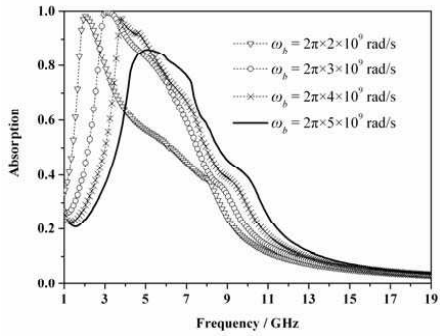

(e)

Figure 7. Normalized power versus wave frequency for different cyclotron frequency. (a) Normalized reflected power of co-polarization: P_{r_co}. (b) Normalized reflected power of cross-polarization: P_{r_cross}. (c) Normalized transmitted power of co-polarization: P_{t_co}. (d) Normalized transmitted power of cross-polarization: P_{t_cross}. (e) Normalized absorbed power: P_a.

curvy fluctuations appearing in Figures 7(a) and (b) are expected as f_b varies in a certain range, which has been confirmed by the numerical experiment introduced in [12] where the reflection coefficient of EM waves from a homogeneous magnetized plasma begins to oscillate as the applied magnetic field goes above a certain value and the oscillation trends are affected obviously by the electron density and the external magnetic field. The multiple irregular peaks of P_{r_co} and P_{r_cross} may be caused by the multiple resonances of type II waves when f_b grows up, and these resonances are mainly influenced by the complicated relationships among incident wave, electron density distribution and the strength of the external magnetic field [30].

It can be found from Figures 7(c) and (d) that with a certain cyclotron frequency, the relationship between P_{t_co} or P_{t_cross} and incidence frequency is similar to that as depicted in Figures 5(c) or (d). However, the turning frequency point for P_{t_co} and the optimum frequency where P_{t_cross} arrives at the maximum are not only affected by the plasma density distribution, but also in great dependence on the cyclotron frequency. Generally, they become higher with the increase of the cyclotron frequency, and their growth magnitude is about the same as that of the cyclotron frequency. Furthermore, within the frequency band ranging from 1 GHz to the turning point, the peak value of P_{t_co} and the corresponding frequency will increase as the cyclotron frequency grows. When the frequency exceeds over the turning point,

the larger the cyclotron frequency is, the more slowly P_{t_co} grows up toward 1, and smaller P_{t_co} can be got at the same frequency. As for P_{t_cross}, the maximum value will increase with increasing the cyclotron frequency f_b, but another small peak will be generated near the main peak when f_b becomes large enough such as over 4 GHz. In addition, with a certain power level, the frequency bandwidth of P_{t_cross} becomes wider as f_b increases.

It is shown in Figure 7(e) that, with a specified cyclotron frequency f_b, the variation trend of the absorbed power P_a with the incidence frequency is similar to that shown in Figures 5(e) or 6(e). On the other hand, it is shown that there is the optimum electron cyclotron frequency (e.g., $f_b = 3$ GHz in this case) at which the EM wave energy has been absorbed most severely by the plasma.

3.6. Propagation and Polarization Characteristics Affected by Magnetic Declination Angle

As the density $N_{e0} = 7.94 \times 10^{17}\ \mathrm{m}^{-3}$, the cyclotron angular frequency $\omega_b = 2\pi \times 3 \times 10^9$ rad/s, the collision frequency $\nu_{en} = 1$ GHz, and the magnetic declination angle θ_B are set respectively as 0°, 30°, 45°, 60°, 90°, the reflected and transmitted powers of co-polarization and cross-polarization as well as the absorbed power are computed and drawn in Figure 8. An interesting phenomenon can be found from these results that P_{r_cross} and P_{t_cross} vanish within the entire frequency band when θ_B is 90°, as shown in Figures 8(b) and (d). In this case, only X-wave which has no E_x component can be generated, and no transformation of EM wave polarization is produced in the process of normal wave incidence on the plasma slab, which leads to the fact that the reflected or transmitted power of cross-polarization is zero.

Figure 8(a) shows that whatever the magnetic declination angle is, there is a turning point around the cyclotron frequency at which P_{r_co} comes to extreme small value. And generally, P_{r_co} increases with the increase of θ_B within most of the frequency range. Furthermore, when the incidence frequency exceeds the turning point, P_{r_co} will increase firstly then decrease gradually, which exists only one peak, as θ_B is no less than 45°, but the curves of P_{r_co} have some fluctuations when θ_B is low than 45°. Figure 8(b) indicates that, within the narrow frequency band where the cyclotron frequency resides, there is a sudden change for P_{r_cross} and rather small values of P_{r_cross} can be obtained. And within the frequency range of 4.9–8.5 GHz, P_{r_cross} increases with the decrease of θ_B. But for other frequency ranges, the P_{r_cross} variation regularity with the θ_B appears fall into chaos. The irregular reflection peaks appearing in Figures 8(a) and (b) also may be caused by the complex factors such as electron density distribution, the strength of

the external magnetic field and the magnetic declination angle, which bring on multiple resonances of type II waves [30].

Regarding Figures 8(c) and (d), it is easy to find that when θ_B is specified, the variance trends in P_{t_co} and P_{t_cross} are similar to that shown in Sections 3.3–3.6, except the cases with θ_B of 90°. However, the influences of different θ_B on P_{t_co} and P_{t_cross} are still obvious. Considering about P_{t_co} firstly, within the frequency band ranging from 1 GHz to the turning point, there is a small peak for P_{t_co} when θ_B is not equal to 90° (the small peak will vanish as θ_B turns to 90°), and the peak value will increase as θ_B reduces, but the corresponding frequency does not change visibly (only increasing a little). When the frequency exceeds over the turning point, the larger θ_B is, the faster P_{t_co} grows up toward 1, and larger P_{t_co} can be got at the same frequency. As for P_{t_cross} with a θ_B of less than 90°, the maximum value and the corresponding frequency will increase as θ_B decreases, and the frequency bandwidth of P_{t_cross} will become wider with a smaller θ_B based on the same transmitted power level.

It can be seen from 8(e) that the relationship between normalized

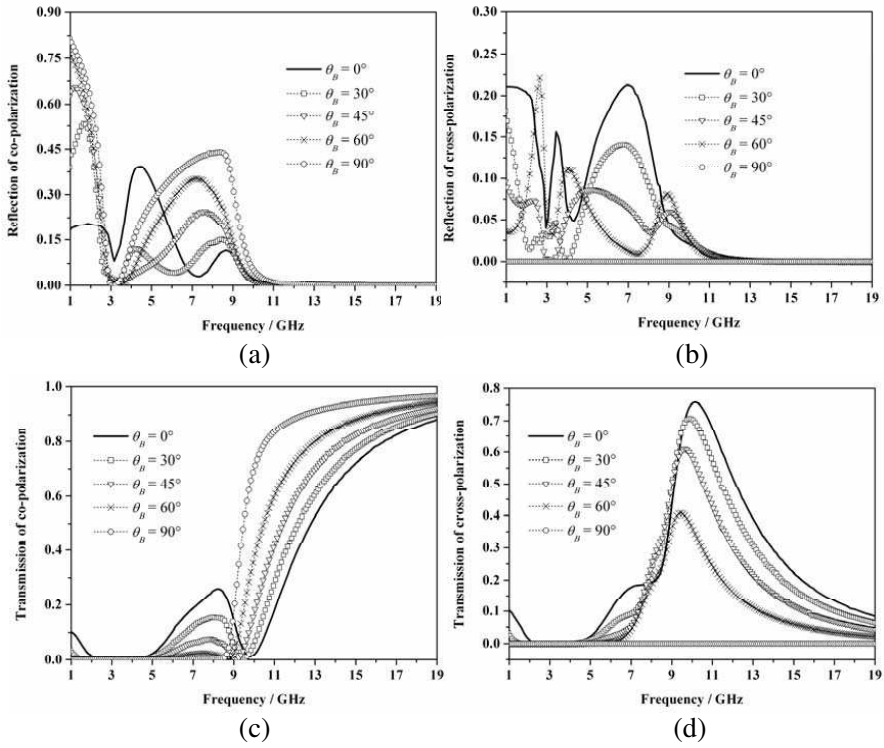

(a) (b)

(c) (d)

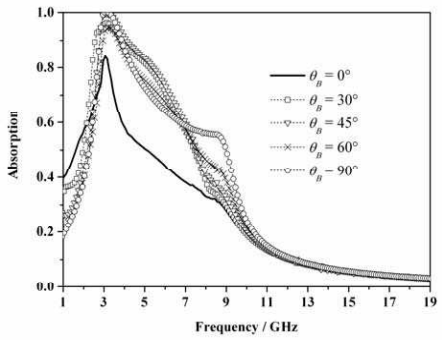

(e)

Figure 8. Normalized power versus wave frequency for different magnetic declination angle θ_B. (a) Normalized reflected power of co-polarization: P_{r_co}. (b) Normalized reflected power of cross-polarization: P_{r_cross}. (c) Normalized transmitted power of co-polarization: P_{t_co}. (d) Normalized transmitted power of cross-polarization: P_{t_cross}. (e) Normalized absorbed power: P_a.

absorbed power P_a and incidence frequency also possesses a similar variation trend to that shown in Sections 3.3–3.6 in spite of arbitrary magnetic declination angle. However, the peak value variation regularity is inconsistent with that of θ_B, and different θ_B (except 0°) imposes no obvious influence on the absorption bandwidth. Moreover, the maximum value of P_a and the corresponding absorption bandwidth with θ_B of 0° will decrease to a great degree compared to that with θ_B of above 0°.

4. CONCLUSION

An analytical technique named propagator matrix method (PMM) is presented to study the propagation and polarization characteristics of EM waves through nonuniform magnetized plasma slab with arbitrary magnetic declination angle. The PMM is confirmed to be a more accurate and efficient tool as compared to the FDTD methods such as that shown in [20]. Moreover, PMM can be used to effectively deal with the phenomenon of strong transformation of EM wave polarization caused by anisotropic magnetized plasma, while other analytical methods such as SMM provided in [15, 17] seem impossible to fulfill this purpose. In the case of TE wave normal incidence on the plasma slab, the reflected or transmitted waves are composed of two kinds of waves, viz., the co-polarized wave and the cross-

polarized wave. The effects of varying four factors (i.e., the electronic density, the collision frequency, the cyclotron frequency and the magnetic declination angle) on the reflected and transmitted powers of co-polarization and cross-polarization, as well as the absorbed power for the typical bi-exponential profile are investigated at length. Consequently, some important conclusions are obtained, which are shown as follows:

(1). The nonuniform magnetized plasma with arbitrary magnetic declination angle ($0^\circ \leq \theta_B < 90^\circ$) exhibit a strong transformation of EM wave polarization when the incident wave normally propagates through the plasma slab. The magnitude of transformation depends on all factors considered here. Generally, P_{t_cross} is larger than P_{r_cross} as a whole within the entire frequency band under the same conditions.

(2). When the magnetic declination angle is set as 90°, the phenomenon of the transformation of EM wave polarization vanishes in the case of normal wave incidence on the plasma slab.

(3). There is a frequency band around the plasma cyclotron frequency where the reflected powers of co-polarization and cross-polarization reach minimum or rather small values. The variation of P_{r_co} or P_{r_cross} with incidence frequency is regular as the peak density N_{e0} or the collision frequency changes. However, the P_{r_co} or P_{r_cross} variation regularity with incidence frequency is more complicated and appears fall into chaos at some frequency ranges, as the cyclotron frequency or the magnetic declination angle θ_B varies.

(4). There exists a turning frequency point for the transmitted power of co-polarization P_{t_co} which is mainly determined by the density distribution and the cyclotron frequency. When incidence frequency increases from 1 GHz to the turning point, P_{t_co} grows up very slowly and a small peak shows. When the frequency increases over this turning point, P_{t_co} increases quickly and then goes to 1 gently, and the increment speed is markedly affected by the four factors mentioned above.

(5). There is an optimum incidence frequency at which the transmitted power of cross-polarization P_{t_cross} reaches a maximum value. This maximum value and the corresponding incidence frequency increases with increasing the density N_{e0} and the cyclotron frequency and reducing the magnetic declination angle (except 90°). Moreover, with the decrease of the collision frequency, the maximum value increases distinctly but the corresponding frequency has almost no changes. For a certain power level, the bandwidth of P_{t_cross} is an increasing function of the peak density N_{e0} and the cyclotron frequency and is in reverse proportion to the collision frequency and the magnetic declination angle (except 90°).

(6). The absorbed power comes to maximum when the incidence frequency matches the cyclotron frequency of the plasma slab, and the maximum value obviously depends on a proper choice of the cyclotron frequency and the magnetic declination angle and is nearly not affected by the peak density N_{e0} and the collision frequency considered here. Moreover, the absorption bandwidth increases with the increase of peak density N_{e0} and the collision frequency and is irregularly affected by the cyclotron frequency and the magnetic declination angle.

This study may be used as the basis for designing tunable devices or stealth apparatus such as plasma transformers of polarization, controlled by a laser light, carriers injection, external applied biasing magnetic field or by variations of the magnetic declination angle. Moreover, some implications obtained from the results can be used to improve communication performance for radar wave through plasma sheath induced by hypersonic space re-entry vehicles, based on the 'magnetic window' technology. From the point of view of enhancing transmission, besides an optimum choice of the plasma parameters such as the electron density and the strength of the background magnetic field, comprehensive utilization of different polarization characteristics of scattered EM signals are needed. Because available literatures about the same topic are few and most of the research results in these areas are classified, no experimental or observational evidence can be found to make a comparison with the results provided in this work. Further investigation will be emphasized on correlative experiments to study the propagation and polarization characteristics of EM waves through nonuniform magnetized plasma generated at the laboratory.

ACKNOWLEDGMENT

This study was supported by the National Natural Science Foundation of China for Grant 40974092.

REFERENCES

1. Hambling, D., "Plasma stealth," *New Scientist*, Vol. 168, No. 2264, 60–61, 2000.
2. Mao, L.-X., H. Zhang, and C.-X. Zhang, "Analysis on the reflection characteristic of electromagnetic wave incidence in closed non-magnetized plasma," *Journal of Electromagnetic Waves and Applications*, Vol. 22, 2285–2296, 2008.
3. Mao, L. X., H. Zhang, Z. Li, and C.-X. Zhang, "Analysis on the stealth characteristic of two dimensional cylinder

plasma envelopes," *Progress In Electromagnetics Research Letters*, Vol. 13, 83–92, 2010.

4. Alexef, I., T. Anderson, and S. Parameswaran, "Experimental and theoretical results with plasma antennas," *IEEE Transactions on Plasma Science*, Vol. 34, No. 2, 166–172, 2006.
5. Wu, X. P., J.-M. Shi, Z. S. Chen, and B. Xu, "A new plasma antenna of beam-forming," *Progress In Electromagnetics Research*, Vol. 126, 539–553, 2012.
6. Kumar, V., M. Mishra, and N. K. Joshi, "Study of a Fluorescent tube as plasma antenna," *Progress In Electromagnetics Research Letters*, Vol. 24, 17–26, 2011.
7. Naz, M. Y., A. Ghaffar, N. U. Rehman, S. Naseer, and M. Zakaullah, "Double and triple Langmuir probes measurements in inductively coupled nitrogen plasma," *Progress In Electromagnetics Research*, Vol. 114, 113–128, 2011.
8. Naz, M. Y., A. Ghaffar, N. U. Rehman, M. Azam, S. Shukrullah, A. Qayyum, and M. Zakaullah, "Symmetric and asymmetric double Langmuir probes characterization of radio frequency inductively coupled nitrogen plasma," *Progress In Electromagnetics Research*, Vol. 115, 207–221, 2011.
9. Wu, C.-J., T.-J. Yang, C. C. Li, and P. Y. Wu, "Investigation of effective plasma frequencies in one-dimensional plasma photonic crystals," *Progress In Electromagnetics Research*, Vol. 126, 521–538, 2012.
10. Hartunian, R. A., G. E. Stewart, S. D. Fergason, T. J. Curtiss, and R. W. Seibold, "Causes and mitigation of radio frequency (RF) blackout during reentry of reusable launch vehicles," Aerosp. Corp., El Segundo, CA, Contractor Rep. ATR-2007(5309)-1, 2007.
11. Gilllman, E. D., J. E. Foster, and I. M. Blankson, "Review of leading approaches for mitigating hypersonic vehicle communications blackout and a method of ceramic particulate injection via cathode spot arcs for blackout mitigation," NASA, Washington DC, NASA/TM-2010-216220, 2010.
12. Manningm, R. M., "Analysis of electromagnetic wave propagation in a magnetized re-entry plasma sheath via the Kinetic equation," NASA, Glenn Research Center, Cleveland, Ohio, NASA/TM-2009-216096, 2009.
13. Liu, J.-F., X.-L. Xi, G.-B. Wan, and L.-L. Wang, "Simulation of electromagnetic wave propagation through plasma sheath using the moving-window finite-difference time-domain method," *IEEE Transactions on Plasma Science*, Vol. 39, No. 3, 852–855, Mar. 2011.

14. Shi, L., B. Guo, Y. Liu, and J. Li, "Characteristic of plasma sheath channel and its effect on communication," *Progress In Electromagnetics Research*, Vol. 123, 321–336, 2012.
15. Hu, B. J., G. Wei, and S. L. Lai, "SMM analysis of reflection, absorption, and transmission from nonuniform magnetized plasma slab," *IEEE Transactions on Plasma Science*, Vol. 27, No. 4, 1131–1135, 1999.
16. Petrin, A. B., "Transmission of microwaves through magnetoactive plasma," *IEEE Transactions on Plasma Science*, Vol. 29, No. 3, 471–478, 2001.
17. Soliman, E. A., A. Helaly, and A. A. Megahed, "Propagation of electromagnetic waves in planar bounded plasma region," *Progress In Electromagnetics Research*, Vol. 67, 25–37, 2007.
18. Huang, H., Y. Fan, B.-I. Wu, F. Kong, and J. A. Kong, "Surface modes at the interfaces between isotropic media and uniaxial plasma," *Progress In Electromagnetics Research*, Vol. 76, 1–14, 2007.
19. Liu, X., Y. Shi, P. Zhu, Y. Zhang, and Q. Yang, "Total internal reflection of pulsed light beam upon ideal non-absorbing plasma," *Journal of Modern Optics*, Vol. 59, No. 7, 643–649, Apr. 2012.
20. Yin, X., H. Zhang, H.-Y. Xu, and X.-F. Zeng, "Improved shift-operator FDTD method for anisotropic magnetized plasma with arbitrary magnetic declination," *Progress In Electromagnetics Research B*, Vol. 38, 39–56, 2012.
21. Yin, X., H. Zhang, Z.-W. Zhao, and S.-J. Sun, "A high efficient SO-FDTD method for magnetized collisional plasma," *Journal of Electromagnetic Waves and Applications*, Vol. 26, Nos. 14–15, 1911–1921, 2012.
22. Yin, X., H. Zhang, et al., "Analysis of the Faraday rotation in a magnetized plasma," *2012 International Conference on Microwave and Millimeter Wave Technology, (ICMMT)*, Vol. 2, 1–4, May 2012.
23. Sodha, M. S., S. K. Mishra, and S. K. Agarwal, "Nonlinear propagation, self-modulation, and faraday rotation of electromagnetic beams in the ionosphere," *IEEE Transactions on Plasma Science*, Vol. 37, No. 2, 375–386, Feb. 2009.
24. Jandieri, G. V., A. Ishimaru, V. Jandieri, and N. N. Zhukova, "Depolarization of metric radio signals and the spatial spectrum of scattered radiation by magnetized turbulent plasma slab," *Progress In Electromagnetics Research*, Vol. 112, 63–75, 2011.
25. Bakunov, M. I. and S. N. Zhukov, "Transformation of

electromagnetic wave polarization by the resonance in a thin solid-plasma film," *Journal of Electromagnetic Waves and Applications*, Vol. 10, No. 6, 791–802, 1996.

26. Negi, J. G. and R. N. Singh, "Propagator matrix formulation of heat transfer in spherically stratified media," *Pure and Applied Geophysics*, Vol. 70, No. 1, 74–80, 1968.
27. Rokhlin, S. I. and L. Wang, "Stable recursive algorithm for elastic wave propagation in layered anisotropic media: Stiffness matrix method," *J. Acoust. Soc. Am.*, Vol. 112, 822–834, 2002.
28. Chew, W. C., *Waves and Fields in Inhomogeneous Media*, Chapter 2, Van Nostrand Reinhold, New York, 1990.
29. Golub, G. H., "Some modified matrix eigenvalue problems," *SIAM Review*, Vol. 15, No. 2, 318–334, 1973.
30. Ginzburg, V. L., *The Propagation of Electromagnetic Waves in Plasmas*, 2nd edition, Chapter 6, Pergamon, New York, 1970.